Ballistic Hall Photovoltammetry of Magnetic Resonance in Individual Nanomagnets

Alain Nogaret,[1,*] Maksym Stebliy,[2] Jean-Claude Portal,[3] Harvey E. Beere,[4] and David A. Ritchie[4]
[1]Department of Physics, University of Bath, Bath BA2 7AY, United Kingdom
[2]School of Natural Sciences, Far Eastern Federal University, Vladivostok 690091, Russia
[3]High Magnetic Field Laboratory, Centre National de la Recherche Scientifique, 25 Avenue des Martyrs, Grenoble 38042, France
[4]Cavendish Laboratory, J.J. Thomson Avenue, Cambridge CB3 0HE, United Kingdom

(Received 17 June 2018; revised 20 March 2021; accepted 26 April 2021; published 20 May 2021)

We report on ballistic Hall photovoltammetry as a contactless probe of localized spin excitations. Spins resonating in the near field of a two-dimensional electron system are shown to induce a long range electromotive force that we calculate. We use this coupling mechanism to detect the spin wave eigenmodes of a single ferromagnet of sub-100 nm size. The high sensitivity of this detection technique, $380\,\mathrm{spins}/\sqrt{\mathrm{Hz}}$, and its noninvasiveness present advantages for probing magnetization dynamics and spin transport.

DOI: 10.1103/PhysRevLett.126.207701

Electrically detected spin resonance is a pivotal technique for probing the spin excitations of the nanosized ferromagnets [1–8] that underpin the coding of information in magnonic crystals [9,10]. The anisotropic magnetoresistance [11] and anomalous Hall effect [1] are examples of nonlinear mechanisms that convert the oscillations of magnetic moments into a dc voltage. The use of a high mobility two-dimensional electron system (2DES) as a photodetector of stray magnetic fields [8,12–17] creates new opportunities for probing localized spin resonances contactlessly in magnetic volumes smaller than the wavelength of light [5,6,18,19] with a sensitivity comparable to superconducting detection [20,21]. The mechanism by which near-field magnetic oscillations induce an electromotive force (emf), however, remains unclear. First, a 2D photodetector experiences zero net magnetic flux when a ferromagnet is placed in its proximity. This *a priori* suggests that any emf is local. Second, most physical quantities, including magnetization and currents, vanish under time averaging.

Here, we investigate the dipolar interactions of magnetic moments oscillating at microwave frequencies with a 2DES. We demonstrate that inductive coupling produces a long range emf in the 2DES. We experimentally observe this emf in a modulation doped $\mathrm{GaAs}/\mathrm{Al}_{.33}\mathrm{GaAs}$ quantum well and use it to measure the spin wave eigenmodes of a single cobalt bar or disk of sub-100 nm size. The photovoltage originates from the breaking of rotational symmetry by the magnetization whose vector components oscillate at different frequencies in the directions parallel and perpendicular to the Larmor magnetic field. The emf is found to be proportional to $\langle M_\mu \dot{M}_\nu - M_\nu \dot{M}_\mu \rangle$, $\{\mu,\nu\} \equiv \{x,y,z\}$, which does not cancel under time averaging as magnetization components M_x, M_y, and M_z oscillate at different frequencies of precession, nutation [22], or ensemble-average Rabi cycling [23]. These frequencies are mixed and rectified by the Hall effect. We obtain a theoretical expression for the emf in the form of a Hall rectified Lenz law. The surface integral of the magnetic flux gives the strength of the dipolar interaction. Ballistic Hall photovoltammetry has a high detection sensitivity of $380\,\mathrm{spins}/\sqrt{\mathrm{Hz}}$, which arises from the emf being proportional to the very high mobility of 2D electrons. Electrically detected spin resonance spectra are compared to micromagnetic simulations.

We synthesized hybrid structures consisting of a single cobalt nanomagnet at the center of a semiconductor Hall bar [Fig. 1(a)]. The heterojunction hosting the 2DES was set 30 nm below the surface. The nanomagnets were fabricated through a combination of precision electron beam lithography and lift-off of a 30 nm cobalt film deposited by magnetron sputtering. Preliminary quantum transport measurements gave the electron mobility $\mu = 1.3 \times 10^6\ \mathrm{cm^2\,V^{-1}\,s^{-1}}$ (4.2 K) and areal electron density $n_s = 1.6 \times 10^{11}\ \mathrm{cm^{-2}}$. The applied magnetic field B_a was then rotated in the plane of the 2DES so that the only perpendicular magnetic field was the normal component of the fringing field. B_a was used to magnetize the bar magnet in the x–y plane. B_a and the local demagnetizing field set the precession frequency of magnetic moments. We studied magnetic resonance over the 36–118 GHz bandwidth using three backward wave oscillators covering the Q, V, and W bands. An overmoded circular waveguide terminated by a linear polarizer was used to guide microwaves to the sample space of a superconducting magnet. The polarizer aligned the microwave magnetic field parallel to the long axis of the nanomagnet [Fig. 1(a)]. The amplitude of the

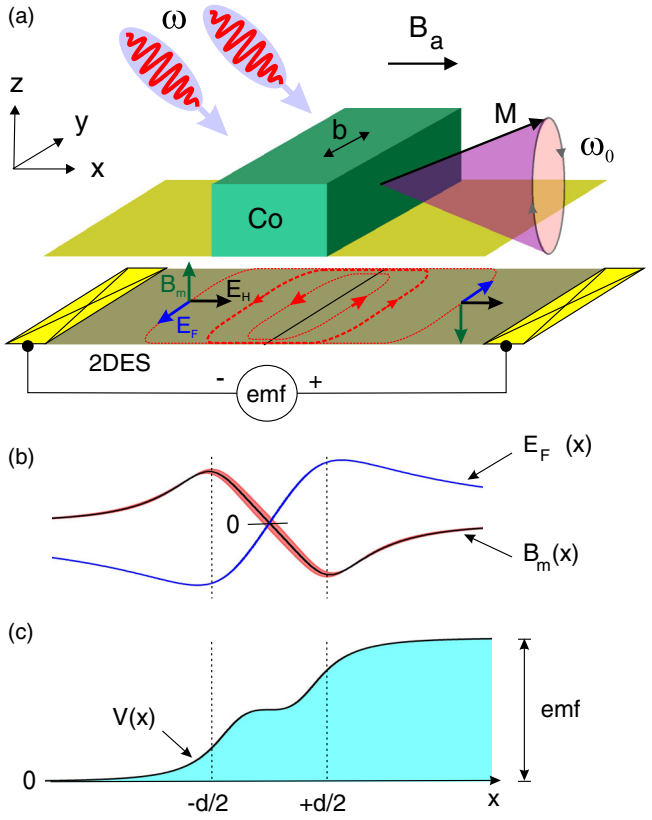

FIG. 1. Principle of ballistic Hall photovoltammetry. (a) A micromagnet (Co) modulates a 2DES with a stray magnetic field, $B_m(x)$. The external magnetic field B_a magnetizes the bar magnet in the plane of the 2DES—either along the short or the long axis. Microwaves (ω, b) drive oscillations of the magnetization M and subsequently of the magnetic modulation B_m and of the induction electric field E_F. Eddy current loops form in the 2DES (red dashed line). These currents are deflected by the Hall effect through electric field $E_H \propto \langle E_F B_m \rangle$, which gives a longitudinal emf. (b) Spatial variation of $B_m(x)$ and $E_F(x)$. (c) Spatial variation of the photovoltage $V(x) = -\int d\chi E_H(\chi)$ across the magnetically modulated 2DES. Device dimensions: magnet height $h = 30$ nm, width $d = 100$ nm, depth of 2DES $z_0 = 30$ nm. ω_0 is the angular frequency of the Larmor precession.

microwave magnetic field on the sample surface was $b \approx 10^{-5}$ T, as deduced from the 0.5 mW microwave power output by the source through a 5.7 mm × 2.9 mm waveguide section. Attenuation was −3 dB, and power losses were negligible. Microwave power was modulated at 830 Hz. We measured the emf induced across a 8 μm length of the 2DES encompassing the nanomagnet [Fig. 1(a)]. Measurements were taken at 1.3 K using lock-in detection.

The principle of ballistic Hall photovoltammetry is schematically described in Fig. 1(a). The fringing field of the bar magnet modulates the 2DES with a spatially varying magnetic field, $B_m(x)$ [Fig. 1(b), black line]. Time dependent oscillations of the magnetization induce eddy current loops in the 2DES [Fig. 1(a)], which are driven by the rate of change of the magnetic modulation $\dot{B}_m$. Note that both the magnetic modulation $B_m(x)$ and the induction electric field $E_F(x)$ have asymmetrical profiles with respect to the center of the bar [Fig. 1(b)]. Hence, the modulation field deflects eddy currents in the same direction on both sides of the magnet. The resulting Hall electric field, $E_H(x) \propto E_F(x) \times B_m(x)$, is symmetrical and generates a finite photovoltage, $V(x) = -\int d\chi E_H(\chi)$, across the magnetic element [Fig. 1(c)]. The temporal oscillations of the photovoltage are rectified during magnetic resonance. At resonance, both B_m and E_F become a superposition of signals of different frequencies. For example, the dipolar magnetic field includes a contribution from magnetic poles perpendicular to B_a, which oscillate at the Rabi frequency $\Omega = \mu_B b/\hbar$, and from magnetic poles parallel to B_a, which oscillate at the Larmor frequency ω_0 where μ_B is the Bohr magneton. The resulting Hall electric field is an aperiodic signal with sidebands $\omega_0 \pm \Omega$. The mean value of the photovoltage is therefore finite. In addition, because the amplitude of eddy currents increases with frequency, the photovoltage induced by the eddy current component oscillating at frequency ω_0 does not cancel out the photovoltage induced by eddy currents oscillating at frequency Ω.

We calculate the emf of a 2DES with a single occupied subband. At low magnetic field ($\mu B_m < 1$), the conductivity is weakly affected by radiation [24,25] and hence is

$$\sigma(x,t) = \frac{n_s e\mu}{1+\mu^2 B_m^2}\begin{pmatrix} 1 & \mu B_m \\ -\mu B_m & 1 \end{pmatrix}, \tag{1}$$

where μ depends on B_m through quantum corrections to the conductivity (see the Supplemental Material [26]). μ implicitly depends on x and t through its dependency on B_m. Ohm's law gives the instantaneous current density $\boldsymbol{J}(x,t) = \boldsymbol{\sigma}(x,t)\boldsymbol{E}(x,t)$, where the electric field $\boldsymbol{E}(x,t)$ incorporates the three following contributions: (i) the microwave electric field, $\boldsymbol{e}(t) = e\cos(\omega t)\boldsymbol{e}_x$; (ii) the electric field of Faraday induction, $\boldsymbol{E}_F(x,t)$, due to the rate of change of the modulation field $\partial \boldsymbol{B}_m/\partial t = -\boldsymbol{\nabla} \wedge \boldsymbol{E}_F$; and (iii) the Hall rectified electric field $\boldsymbol{E}_H(x)$.

As no current is injected in the Hall bar, the requirement that $\langle \boldsymbol{J}(x,t) \rangle = 0$ gives the longitudinal and transverse components of $\boldsymbol{E}_H$ as solutions of

$$\begin{cases} \sigma_{\parallel}(x)E_{H,x}(x) + \sigma_{\perp}(x)E_{H,y}(x) = \imath_x(x) \\ -\sigma_{\perp}(x)E_{H,x}(x) + \sigma_{\parallel}(x)E_{H,y}(x) = \imath_y(x), \end{cases} \tag{2}$$

where $\sigma_{\parallel}(x)$, $\sigma_{\perp}(x)$ are the time averaged conductivities and $\imath_x(x)$, $\imath_y(x)$ the time averaged current densities. These local coefficients are calculated in Table I. The nondiagonal conductivity $\sigma_{\perp}$ and the transverse current $\imath_y$ vanish by time averaging. In addition, the spatial dependence of $\imath_y$ is the same as that of the flux of the magnetic modulation; hence, $\imath_y$ also cancels by integration over space. From Eq. (2), the

TABLE I. Local time averaged conductivities and currents.

$\sigma_{\parallel}$	$\sigma_{\perp}$	ι_x	ι_y
$\langle\mu/(1+\mu^2 B_m^2)\rangle$	0	$-\langle[\mu^2/(1+\mu^2 B_m^2)]B_m E_F\rangle$	0

Hall electric field only has a longitudinal component: $E_H(x) = \iota(x)/\sigma_{\parallel}(x)$ [Fig. 1(a)].

In order to capture the essential physics while keeping the derivation analytical, our model considers the magnetization $\boldsymbol{M}$ to be the average density of magnetic moments. This average incorporates the spin waves formed at the edges and in the bulk of the magnet, which we calculate in detail below. With this approximation, the electric field of Faraday induction is transverse and equal to

$$E_F(x,t) = -\int_{-\infty}^{x} d\xi \mu_0 [\alpha_x(\xi)\dot{M}_x(t) + \alpha_z(\xi)\dot{M}_z(t)], \tag{3}$$

and the stray magnetic field is

$$B_m(x,t) = \alpha_x(x)\mu_0 M_x(t) + \alpha_z(x)\mu_0 M_z(t), \tag{4}$$

whose spatial variation is given by the form factors [14]

$$\begin{aligned}\alpha_x(x) &= -\frac{1}{2\pi}[g_0^+(x) - g_0^-(x) - g_h^+(x) + g_h^-(x)]\\ \alpha_z(x) &= -\frac{1}{2\pi}[f_0^+(x) - f_0^-(x) - f_h^+(x) + f_h^-(x)],\end{aligned} \tag{5}$$

where $f_z^{\pm}(x) = \arctan[(x \pm d/2)/(z_0 + z)]$ and $g_z^{\pm}(x) = \ln\sqrt{(z_0+z)^2 + (x \pm d/2)^2}$. d and h are the width and height of the bar magnet, and z_0 is the depth of the 2DES [Fig. 1(a)]. Equations (3)–(5) are exact solutions of Maxwell's equations in both the far field and near field. Inserting $E_F(x,t)$ [Eq. (3)] and $B_m(x,t)$ [Eq. (5)] into $\iota_x(x)$ (Table I), one obtains the Hall rectified electric field $E_H(x)$. The spatial variation of the photovoltage $V(x)$ generated by the Hall electric field follows from space integration as

$$\begin{aligned}V(x) = &\frac{1}{\sigma_{\parallel}}\left\langle\frac{\mu^2\mu_0^2 M_x(t)\dot{M}_z(t)}{1+\mu^2 B_m^2}\right\rangle A_{xz}(x)\\ &+\frac{1}{\sigma_{\parallel}}\left\langle\frac{\mu^2\mu_0^2 M_z(t)\dot{M}_x(t)}{1+\mu^2 B_m^2}\right\rangle A_{zx}(x).\end{aligned} \tag{6}$$

The dipolar field emanating from magnetic pole M_z threads the following area of the 2DES:

$$A_{xz}(x) = \int_{-\infty}^{x} d\xi \int_{-\infty}^{\xi} d\zeta \alpha_x(\xi)\alpha_z(\zeta). \tag{7}$$

The dual area $A_{zx}(x)$, obtained by permutation of indices, is threaded with a field emanating from pole M_x. We have used Eq. (6) to plot the profile of the photovoltage in Fig. 1(c). The emf is obtained by calculating $V(x)$ in the far field ($x \to +\infty$). The effective areas obey the sum rule $A_{xz}(+\infty) + A_{zx}(+\infty) = 0$. As long as the magnetic modulation is not too large ($\mu B_m < 1$), the emf takes this simple form:

$$emf = \mu\mu_0^2 A\langle M_z\dot{M}_x - M_x\dot{M}_z\rangle. \tag{8}$$

This is effectively a Hall rectified Lenz law. The emf is proportional to the rate of change of the magnetic flux created by resonating magnetic moments $\dot{M}_x$ (resp. $\dot{M}_z$). The time averaged term in Eq. (8) cancels off resonance when M_x and M_z oscillate at the same frequency. However, when the system crosses resonance, $\dot{M}_z = \omega_0 M_z$ and $\dot{M}_x = \Omega M_x$, giving a finite emf. The emf is proportional to the strength of dipolar coupling between the magnet and the 2DES through area $A \equiv A_{zx}(+\infty)$, which depends on the magnet dimensions and separation from the 2DES. The emf is also proportional to the electron mobility μ, which can be as high as 36×10^6 cm^2 V^{-1} s^{-1} [51,52] and critically grants exceptional sensitivity to the detection of spin resonance.

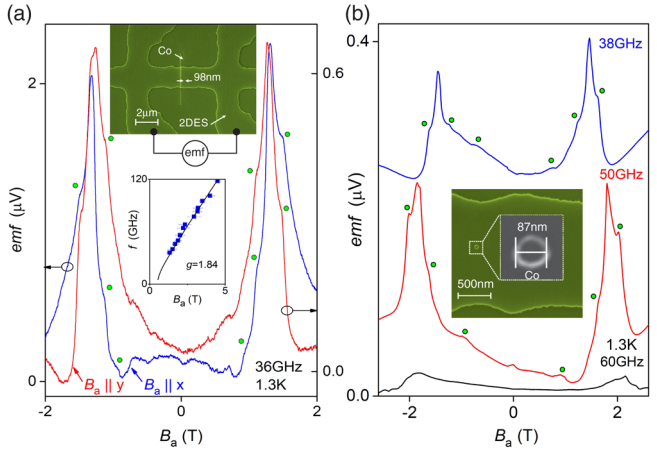

FIG. 2. Photovoltammetry of individual sub-100 nm magnets. (a) Magnetic resonance spectrum of a cobalt bar magnet magnetized along its short axis (blue line) and long axis (red line) at 36 GHz. The volume resonance of magnetic moments gives the main peak. Kinks in the photovoltage spectrum (dot symbols) arise from spin excitations localized at the edges of the bar. Top inset: cobalt bar magnet of cross section $d \times h = 98\ \text{nm} \times 30\ \text{nm}$ fabricated at the surface of a 2 μm wide GaAs/AlGaAs Hall bar. Lower inset: frequency dispersion of the main resonance for $B_a \| x$ (square symbols) and predicted (full line). (b) Resonance spectrum of a cobalt disk at 38, 50, and 60 GHz. Inset: cobalt disk of diameter $\varnothing = 87$ nm and height $h = 30$ nm on a Hall bar.

Figures 2(a) and 2(b) show the magnetic resonance spectra that we obtained by measuring the emf across a single cobalt bar magnet and a sub-100 nm disk, respectively. The position of the main resonance follows the frequency dispersion predicted by Kittel's equation for the

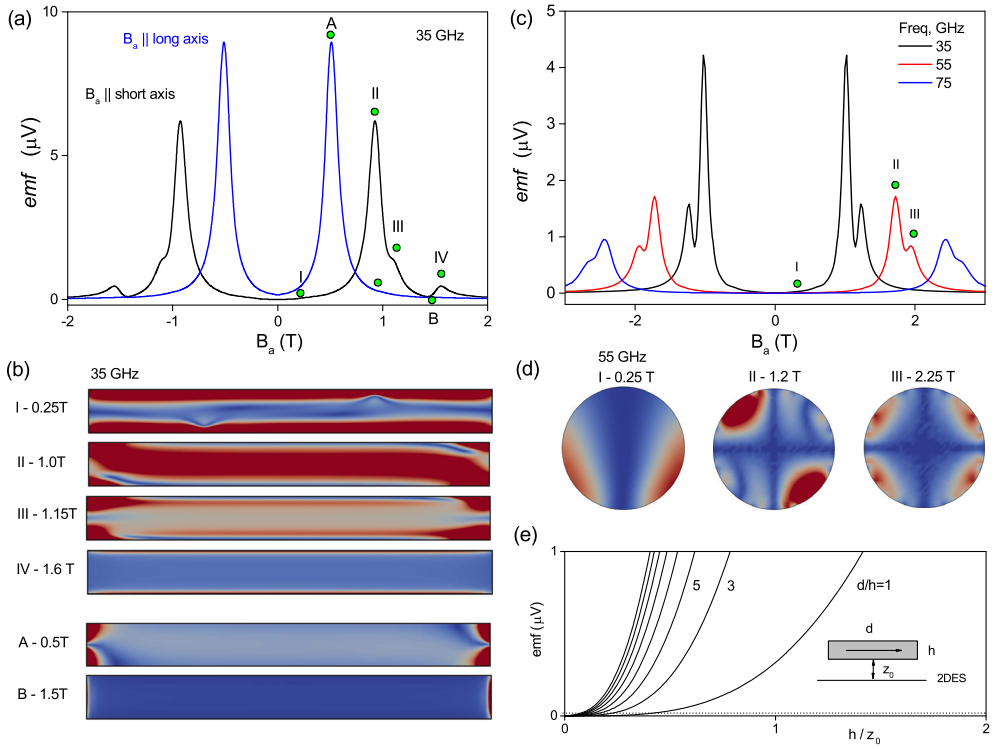

FIG. 3. Theoretical photovoltammetry spectra. (a) emf spectrum of a cobalt bar magnet of cross section $d \times h = 80\ \text{nm} \times 30\ \text{nm}$ when the magnetization is either along the short axis (black line) or the long axis (blue line). (b) Maps of the local amplitudes of magnetic moment oscillations corresponding to the emf peaks I–IV and A–B. (c) emf spectrum of a cobalt disk of diameter $\varnothing = 80$ nm and height $h = 30$ nm. (d) Spin wave eigenmodes corresponding to the emf peaks I–III. (e) Dependence of the emf on the dimensions of a bar magnet of constant cross section. Parameters: cobalt saturation magnetization, $\mu_0 M_s = 1.8$ T; Gilbert damping, $\alpha = 0.05$; exchange interaction constant, $A = 30 \times 10^{-12}$ J/m.

bar when shape anisotropy dominates over magnetocrystalline anisotropy ($B_a \| x$) [26]. When $B_a \| y$, the reverse occurs and, although the resonance does shift to a lower magnetic field, this shift is smaller than that anticipated from shape anisotropy alone. For example, at 36 GHz [Fig. 2(a)], the peak shifts from 1.35 T ($B_a \| x$) to 1.15 T ($B_a \| y$), instead of the predicted 0.55 T, due to magnetocrystalline anisotropy pinning the resonance position at 1.05 T [26]. The emf spectra of the Co bar and disk [Fig. 2(b)] show a fine structure superimposed on the main peak (circle symbols) that follows the same frequency dispersion as the main peak [26]. The small amplitude of kinks suggests low-dimensional spin waves quantized by the inhomogeneous dipolar field near the poles [5,6,53]. The ability to inductively detect these local resonances, which involve of a few hundred thousand Bohr magnetons, relies on the long-lived eddy currents of ballistic electrons. This implies magnet sizes smaller than the electron mean free path and Hall bars narrower than the mean free path to minimize thermalization of eddy currents between the Co disk and Hall bar edges.

In order to test our theory, we performed micromagnetic calculations of the emf for both magnet geometries. These calculations are intended to predict qualitative features of the resonant peaks rather than the exact peak positions as magnetocrystalline anisotropy of polycrystalline cobalt and interfacial magnetoelastic effects were not included [26]. We computed the magnetization as a time series using MUMAX^3 [54] and inserted this in Eq. (8) to obtain the emf. The magnetic volume was partitioned into 5 nm × 5 nm cells for the bar and 2 nm × 2 nm cells for the disk to resolve the dipolar-exchange spin waves localized at the edges. The magnetic field B_a was varied in the range $-4\ \text{T} \rightarrow +4\ \text{T}$ in steps of 25 mT. During each step, a microwave magnetic field $b = 10^{-5}$ T was applied, and the time dependence of the magnetization was calculated [26]. The instantaneous magnetization was obtained by averaging the magnetic moments in each cell. The $M_x(t)$ and $M_z(t)$ time series data were inserted in Eq. (8) to calculate the emf and its dependence on B_a. Time averaging was weighted by probability $e^{-t/\tau}$ that Hall voltage oscillations remain coherent at time t. The damping rate $\tau^{-1} = \tau_\gamma^{-1} + \tau_\mu^{-1}$ compounded the Gilbert damping time of the magnetization, $\tau_\gamma = (\alpha\gamma M_s)^{-1} \approx 63$ ps, with the decay time of eddy currents $\tau_\mu = m^*\mu/e \approx 48$ ps. $\alpha = 0.05$ is Gilbert's damping (Co), γ is the gyromagnetic ratio, and e and m^* are the electron charge and effective mass, respectively.

The calculated emf spectra are shown in Fig. 3. Resonance in the bulk of the bar magnet [Fig. 3(a)] gives a resonance peak (peak A) that shifts from 0.5 T to 0.95 T (peak II) as the magnetization rotates from the long axis to the short axis. The theoretical spectra exhibit a series of satellite peaks (I–III–IV) as in experiments. These peaks correspond to spin wave eigenmodes confined near the poles by the wells of a demagnetizing field [Fig. 3(b)] [6,53]. These modes are increasingly localized as B_a increases [5]. A distinguishing feature of the cobalt disk [Fig. 3(c)] is the subsidiary peak (peak III) after the main resonance (peak II), also observed in experiments. Simulations ascribe peaks II and III to the dipolar and quadrupolar spin wave eigenmodes plotted in Fig. 3(d).

Figure 3(e) shows the dependence of the emf on the strength of dipolar coupling between the magnet and the 2DES as a function of h/z_0 for bar magnets of different aspect ratios d/h. Smaller 2DES-magnet separations or thicker magnets increase the emf. For our disk of dimensions $h = z_0 = 30$ nm and radius $= 43$ nm, we estimate the detection sensitivity to be $380\,\mathrm{spins}/\sqrt{\mathrm{Hz}}$ [26]. This sensitivity is comparable to that of quantum circuits at mK temperatures, $65\,\mathrm{spins}/\sqrt{\mathrm{Hz}}$ [20,21], while our detection method retains the versatility of less sensitive induction methods, $\approx 10^{10}\,\mathrm{spins}/\sqrt{\mathrm{Hz}}$ [27]. Other techniques such as the photoionization of nitrogen vacancies in diamond [55] or Coulomb blockaded quantum dots [56–58] achieve greater spin detection sensitivities but are less versatile. The emf detected with the present technique varies as a square root of microwave power, as expected from Eq. (8) [26]. This is in contrast to the power dependence of spin rectification by anisotropic magnetoresistance effects, which is linear [1].

We have observed magnetic resonance in the photovoltage at temperatures between 1.3 and 85 K [26]. Photodetected spin resonance may be observed at even higher temperatures using nonpolar 2D materials such as graphene that have high mobility at room temperature [52]. In summary, ballistic Hall photovoltammetry is a noninvasive and sensitive probe that has significant advantages for studying local spin dynamics.

This research was supported by the European Union FP7 IRSES 318973.

*Corresponding author.
A.R.Nogaret@bath.ac.uk

[1] M. Harder, Y. Gui, and C. M. Hu, Phys. Rep. **661**, 1 (2016).
[2] Y. S. Gui, S. Holland, N. Mecking, and C. M. Hu, Phys. Rev. Lett. **95**, 056807 (2005).
[3] S. T. B. Goennenwein, S. W. Schink, A. Brandlmaier, A. Boger, M. Opel, R. Gross, R. S. Keizer, T. M. Klapwijk, A. Gupta, H. Huebl, C. Bihler, and M. S. Brandt, Appl. Phys. Lett. **90**, 162507 (2007).
[4] A. A. Awad, G. R. Aranda, D. Dieleman, K. Y. Guslienko, G. N. Nakazei, B. A. Ivanov, and F. G. Aliev, Appl. Phys. Lett. **97**, 132501 (2010).
[5] J. P. Park, P. Eames, D. M. Engebretson, J. Berezovsky, and P. A. Crowell, Phys. Rev. Lett. **89**, 277201 (2002).
[6] J. Jorzick, S. O. Demokritov, B. Hillebrands, M. Bailleul, C. Fermon, K. Y. Guslienko, A. N. Slavin, D. V. Berkov, and N. L. Gorn, Phys. Rev. Lett. **88**, 047204 (2002).
[7] S. Jain, V. Novosad, F. Y. Fradin, J. E. Pearson, V. Tiberkevich, A. N. Slavin, and S. D. Bader, Nat. Commun. **3**, 1330 (2012).
[8] P. Saraiva, A. Nogaret, J. C. Portal, H. E. Beere, and D. A. Ritchie, Phys. Rev. B **82**, 224417 (2010).
[9] A. V. Chumak, A. A. Serga, and B. Hillebrands, Nat. Commun. **5**, 4700 (2014).
[10] K. Vogt, F. Y. Fradin, J. E. Pearson, T. Sebastian, S. D. Bader, B. Hillebrands, A. Hoffmann, and H. Schultheiss, Nat. Commun. **5**, 3727 (2014).
[11] H. Zhou, X. Fan, F. Wang, C. Jiang, J. Rao, X. Zhao, Y. S. Gui, C. M. Hu, and D. Xue, Appl. Phys. Lett. **104**, 102401 (2014).
[12] A. K. Geim, S. V. Dubonos, J. G. S. Lok, I. V. Grigorieva, J. C. Maan, L. Theil Hansen, and P. E. Lindelof, Appl. Phys. Lett. **71**, 2379 (1997).
[13] D. N. Lawton, A. Nogaret, S. J. Bending, D. K. Maude, J. C. Portal, and M. Henini, Phys. Rev. B **64**, 033312 (2001).
[14] A. Nogaret, J. Phys. Condens. Matter **22**, 253201 (2010).
[15] D. Uzur, A. Nogaret, H. E. Beere, D. A. Ritchie, C. H. Marrows, and B. J. Hickey, Phys. Rev. B **69**, 241301(R) (2004).
[16] A. Nogaret, D. N. Lawton, D. K. Maude, J. C. Portal, and M. Henini, Phys. Rev. B **67**, 165317 (2003).
[17] A. Nogaret, P. Mondal, A. Kumar, S. Ghosh, H. Beere, and D. Ritchie, Phys. Rev. B **96**, 081302(R) (2017).
[18] G. Gubbiotti, S. Tacchi, G. Carlotti, N. Singh, S. Goolaup, A. O. Adeyeye, and M. Kostylev, Appl. Phys. Lett. **90**, 092503 (2007).
[19] U. Ebels, J. L. Duvail, P. E. Wigen, L. Piraux, L. D. Buda, and K. Ounadjela, Phys. Rev. B **64**, 144421 (2001).
[20] A. Bienfait, J. J. Pla, Y. Kubo, M. Stern, X. Zhou, C. C. Lo, C. D. Weis, T. Schenkel, M. L. W. Thewaldt, D. Vion, D. Esteve, B. Julsgaard, K. Mølmer, J. J. L. Morton, and P. Bertet, Nat. Nanotechnol. **11**, 253 (2016).
[21] S. Probst, A. Bienfait, P. Campagne-Ibarcq, J. J. Pla, B. Albanese, J. F. Da Silva Barbosa, T. Schenkel, D. Vion, D. Esteve, K. Mølmer, J. J. L. Morton, R. Heeres, and P. Bertet, Appl. Phys. Lett. **111**, 202604 (2017).
[22] D. Böttcher and J. Henk, Phys. Rev. B **86**, 020404(R) (2012).
[23] A. Capua, C. Rettner, S. H. Yang, T. Phung, and S. P. Parkin, Nat. Commun. **8**, 16004 (2017).
[24] I. A. Dmitriev, M. G. Vavilov, I. L. Aleiner, A. D. Mirlin, and D. G. Polyakov, Phys. Rev. B **71**, 115316 (2005).
[25] A. Nogaret, F. Nasirpouri, J. C. Portal, H. E. Beere, D. A. Ritchie, A. T. Hindmarch, and C. H. Marrows, Europhys. Lett. **94**, 28001 (2011).
[26] See Supplemental Material, which includes Refs [27–50], at http://link.aps.org/supplemental/10.1103/PhysRevLett.126.207701 for frequency dispersion data, anisotropy, and spin sensitivity calculations.

[27] Y. Twig, E. Suhovoy, and A. Blank, Rev. Sci. Instrum. **81**, 104703 (2010).
[28] J. A. C. Bland, R. D. Bateson, P. C. Riedi, R. G. Graham, H. J. Lauter, J. Penfold, and C. Shackleton, J. Appl. Phys. **69**, 4989 (1991).
[29] Y. Z. Wu, H. F. Ding, C. Jing, D. Wu, G. S. Dong, X. F. Jin, K. Sun, and S. Zhu, J. Magn. Magn. Mater. **198**, 297 (1999).
[30] C. Chappert and P. Bruno, J. Appl. Phys. **64**, 5736 (1988).
[31] W. Sucksmith and J. E. Thompson, Proc. R. Soc. **225**, 362 (1954).
[32] R. M. Bozorth, Phys. Rev. **96**, 311 (1954).
[33] R. O'Handley, *Modern Magnetic Materials: Principles and Appplications* (Wiley, Chichester, 2000).
[34] J. C. M. Henning and J. H. den Boef, Appl. Phys. **16**, 353 (1978).
[35] M. Kutz, *Mechanical Engineer's Handbook* (Wiley, New York, 1986).
[36] D. Craik, *Magnetism: Principles and Applications* (Wiley, New York, 1995).
[37] R. I. Cottam and G. A. Saunders, J. Phys. C **6**, 2105 (1973).
[38] J. H. Davies and I. A. Larkin, Phys. Rev. B **49**, 4800 (1994).
[39] G. K. White, Proc. Phys. Soc. London **86**, 159 (1965).
[40] P. Bruno, J. Appl. Phys. **64**, 3153 (1988).
[41] G. Boero, M. Bouterfas, C. Massin, F. Vincent, P. A. Besse, R. S. Popovic, and A. Schweiger, Rev. Sci. Instrum. **74**, 4794 (2003).
[42] Y. Kubo, F. R. Ong, P. Bertet, D. Vion, V. Jacques, D. Zheng, A. Dréau, J. F. Roch, A. Auffeves, F. Jelezko, J. Wrachtrup, M. F. Barthe, P. Bergonzo, and D. Esteve, Phys. Rev. Lett. **105**, 140502 (2010).
[43] Y. Kubo, I. Diniz, C. Grezes, T. Umeda, J. Isoya, H. Sumiya, T. Yamamoto, H. Abe, S. Onoda, T. Ohshima, V. Jacques, A. Dréau, J. F. Roch, A. Auffeves, D. Vion, D. Esteve, and P. Bertet, Phys. Rev. B **86**, 064514 (2012).
[44] K. Klein, B. Hauer, B. Stoib, M. Trautwein, S. Matich, H. Huebl, O. Astakhov, F. Friedhelm, R. Bittl, M. Stutzmann, and M. S. Brandt, Rev. Sci. Instrum. **84**, 103911 (2013).
[45] J. J. Pla, K. Y. Tan, J. P. Dehollain, W. H. Lim, J. J. L. Morton, D. N. Jamieson, and A. S. Dzurak, Nature (London) **489**, 541 (2012).
[46] J. J. Pla, K. Y. Tan, J. P. Dehollain, W. H. Lim, J. J. L. Morton, F. A. Zwanenburg, D. N. Jamieson, A. S. Dzurak, and A. Morello, Nature (London) **496**, 334 (2013).
[47] I. S. Ibrahim, V. A. Schweigert, and F. M. Peeters, Phys. Rev. B **57**, 15416 (1998).
[48] F. M. Peeters and X. Q. Li, Appl. Phys. Lett. **72**, 572 (1998).
[49] B. J. Baelus and F. M. Peeters, Appl. Phys. Lett. **74**, 1600 (1999).
[50] C. W. J. Beenakker and H. van Houten, *Quantum Transport in Semiconductor Nanostructures*, edited by Ehrenreich and Turnbull (Academic Press, New York, 1991), p. 1.
[51] D. G. Schlom and L. N. Pfeiffer, Nat. Mater. **9**, 881 (2010).
[52] J.-H. Chen, C. Jang, S. Xiao, M. Ishigami, and M. S. Fuhrer, Nat. Nanotechnol. **3**, 206 (2008).
[53] C. Bayer, J. Jorzick, S. O. Demokritov, A. N. Slavin, K. Y. Guslienko, D. V. Berkov, N. L. Gorn, M. P. Kostylev, and B. Hillebrands, in *Spin Dynamics in Confined Magnetic Structures III*, edited by B. Hillebrands and A. Thiaville (Springer-Verlag, Berlin, Heidelberg, 2006), Ch. 2, pp. 57–103.
[54] A. Vansteenkiste, J. Leliaert, M. Dvornik, M. Helsen, F. Garcia-Sanchez, and B. Van Waeyenberge, AIP Adv. **4**, 107133 (2014).
[55] F. M. Hrubesch, G. Braunbeck, M. Stutzmann, F. Reinhard, and M. S. Brandt, Phys. Rev. Lett. **118**, 037601 (2017).
[56] A. Morello, J. J. Pla, F. A. Zwanenburg, K. W. Chan, K. Y. Tan, H. Huebl, M. Mottonen, C. D. Nugroho, C. Yang, J. A. van Donkelaar, A. D. C. Alves, D. N. Jamieson, C. C. Escott, L. C. L. Hollenberg, R. G. Clark, and A. S. Dzurak, Nature (London) **467**, 687 (2010).
[57] J. M. Elzerman, R. Hanson, L. H. Willems van Beveren, B. Witkamp, L. M. K. Vandersypen, and L. P. Kouwenhoven, Nature (London) **430**, 431 (2004).
[58] F. H. L. Koppens, C. Buizert, K. J. Tielrooij, I. T. Vink, K. C. Nowack, T. Meunier, L. P. Kouwenhoven, and L. M. K. Vandersypen, Nature (London) **442**, 766 (2006).